

Title Imaging the atomic structure and local chemistry of platelets in natural type Ia diamond

Authors: E.J Olivier*¹, J.H Neethling¹, R.E Kroon², S.R. Naidoo³, C.S Allen^{4,5}, H. Sawada^{4,5,6} P.A. van Aken⁷, and A.I Kirkland^{4,5}

Affiliations:

¹Centre for HRTEM, NMMU, University Way, Summerstrand, Port Elizabeth, South Africa

²Department of Physics, University of the Free State, Bloemfontein, South Africa

³Materials Physics Research Institute, DST-NRF Centre of Excellence in Strong Materials (CoE-SM), School of Physics, University of the Witwatersrand, Private bag 3, Wits 2050, Johannesburg, South Africa

⁴Electron Physical Science Imaging Center, Diamond Light Source Ltd., Didcot, Oxfordshire, OX11 0DE, United Kingdom

⁵Department of Materials, University of Oxford, Parks Road, Oxford, OX1 3PH, United Kingdom

⁶JEOL UK Ltd., JEOL House, Silvercourt, Watchmead, Welwyn garden City, Herts, AL71LT, UK.

⁷Stuttgart Center for Electron Microscopy, Max Planck Institute for Solid State Research, Heisenbergstr. 3, 70569 Stuttgart, Germany

Abstract

The past decades have seen many efforts to characterize {001} platelet defects in type Ia diamond. It is known that N is concentrated at the defect core. However, an accurate description of the atomic structure of the defect and the role that N plays in this is still unknown. Here, we provide experimental evidence that for the first time allows visualization of the atomic arrangement within platelet cores. Using aberration corrected transmission electron microscopy together with electron energy loss spectroscopy obtained we have successfully determined the atomic arrangement within platelet defects in a natural type Ia diamond and matched this to a prevalent theoretical model. The platelet has an anisotropic atomic structure with a zig-zag ordering of defect pairs along the defect line. Electron energy loss near edge fine structure of both C-K and N-K edges obtained from the platelet core show evidence supporting a trigonal bonding arrangement at interstitial sites.

Introduction

Research studying the nature of defects present in diamond has been ongoing for many decades. This is mainly due to the influence of defects in shaping the electronic and optical properties of diamond¹. Exploitation of these properties have been proposed in a number of novel devices such as next generation optical storage, high-frequency field-effect transistors (FETs) and high-power switches^{2,3}. In the case of natural diamonds, the presence and structure of defects within the material allow for accurate determination of the geological environment present during its formation and play an important role in defining a diamond's colour and quality¹. In particular, the role of defects in the interpretation of signal from the industrially important diamond anvil cell (DAC) applications using Type I diamonds have attracted attention⁴. Consequently, it is important to classify these defects in terms of their atomic arrangements and energies of formation.

N is a common impurity found in diamond and is known to form several different types of defect arrangements⁵. In particular, the presence and quantity of N related defects are seen as the

cornerstone of diamond classification⁵. A diamond containing significant concentrations of N is termed “Type I” and these diamonds have absorption bands in their IR spectra related to N. Diamonds that have low concentrations of N do not show absorption features related to N and are classified as “Type II”. In addition, type I diamond is further classified into type Ia or Ib for N present in aggregated form or in isolated substitutional sites within the material, respectively.

In natural type 1a diamonds N aggregates are present with and within extended defects on {001} planes called platelets. Figure 1 (a) shows platelets on (100)_p and (010)_p planes* viewed edge-on and loops on inclined {111} planes with the electron beam along a <110> direction. A single platelet viewed edge-on is shown in Figure 1(b) at higher magnification.

Figure 1

Platelets in diamond were first observed by Raman and Nilakantan in 1940⁶ using X-ray diffraction and later characterized using transmission electron microscopy (TEM) by Evans and Phaal in 1962⁷. Initially the formation of platelets was thought to be due to agglomeration and precipitation of N exclusively. However, some studies challenged this assertion suggesting instead, that the platelets consist of C interstitial complexes.⁸ It is however, generally believed that the interstitial species that ultimately form the platelets arise from a N aggregation process.^{9,10}

The platelet structure has attracted significant attention due to the difficulty in fully characterising the defect as well as explaining the potential role of N in its formation and structure. This is important since there is currently no consensus on the exact mechanism responsible for the formation of platelets. Elucidating this mechanism could provide valuable information needed for the purpose of geophysical dating of natural diamonds and further have implications related to their intended use such as in the case of diamond anvil cells (DAC)⁴ and HPHT treated diamonds.

One of the main difficulties in characterising platelets has been the inability to directly visualize the atomic arrangement within these defects. The main challenge is that a spatial resolution of better than 89 pm has to be achieved in order to resolve the atomic columns of the defect along the <110> directions in diamond as shown in Figure 1(c). This requires a carefully prepared specimen that is sufficiently thin and effectively free from amorphous carbon and any damaged surfaces.

Earlier attempts concentrated on the use of high resolution TEM imaging but direct interpretation was not possible due to inherent difficulties in the interpretation of high resolution phase contrast of defects in thick samples¹⁰. In light of this several structure models have been developed to describe the platelets^{10,11,12,13}. Figures 2 (a) – (d) show the prevalent atomic structure models viewed along the [110]_p and [1-10]_p directions. An anisotropic nature of the platelet atomic structure is seen in Figures 2 (b)-(d). This anisotropy has been reported in many experimental studies^{7,10,14} and is manifest as a small difference in the atomic arrangement along the [110]_p and [1-10]_p directions. Subsequently, this feature has become one of the key characteristics of any proposed platelet model.

Figure 2

Experimental evidence suggested a strong link between N and the structure of platelets¹⁵. A seminal paper by Berger and Pennycook in 1982 provided the first direct evidence of this in {001} platelets in natural type Ia diamonds,¹⁵ initiating the idea that N possibly plays an important role in the formation and structure of platelets¹¹. Using electron energy loss spectroscopy (EELS) in the TEM, Berger and

* In this work (hkl)_p and [uvw]_p refer to planes and directions with respect to the platelet in which the cubic symmetry of the diamond lattice is lowered.

Pennycook clearly showed the presence of an N-K edge in EEL spectra obtained from the cores of several platelet defects.

Experimental data from subsequent studies have also shown the detection of N in measurable quantities in platelets using predominantly EELS^{16, 17, 18}. However, the concentration of N detected varied dramatically, with values between 6% and 61% of a monolayer reported⁹, suggesting N to be an adventitious contaminant rather than constituting an essential component of the structure⁹. The quantities detected are in general also too low for an N only platelet structure and this necessitates the presence of C in the platelet structure¹⁴.

One key observation made by Berger et al. (1982)¹⁵ was a gradual decrease of the N signal with repeated measurements of the same platelet, indicating a possible sensitivity of the platelet to electron beam irradiation.

Modern scanning transmission electron microscopy (STEM) techniques overcome many of the obstacles experienced during previous characterization attempts and in this paper we present for the first time aberration corrected high resolution STEM images of platelets showing the atomic arrangement in the platelet core. This is supported by EELS data obtained from the platelet core that enable a complete description of the platelet structure.

Experimental Methods

The diamond used in this study is a natural type Ia diamond originating from South Africa. Type Ia natural diamonds are known to contain platelets as defects. A focused ion beam (FIB) instrument was used for preparation of a FIB lamella for TEM analysis.

To study the atomic structure and chemical composition of platelets in greater detail, aberration corrected STEM imaging in high angle annular dark field (HAADF) mode was used together with EELS spectrum imaging. Conventional high resolution TEM (HRTEM) images were also recorded (Fig 12-14 in supplementary info). Images were recorded at 200 kV accelerating voltage for most of the data reported but 80 kV imaging was also used to investigate possible effects of electron damage on the platelet structure.

HRTEM (Fig. 14 in supplementary info) and STEM images were qualitatively compared to simulated images generated from the structural models proposed by Lang et al. (1964)¹¹, Humble et al. (1985)¹², Bursill et al. (1981)¹⁴, Miranda et al. (2004)¹³ and Barry et al. (1985)⁹ using the multislice¹⁹ method implemented in the JEMS²⁰ image simulation program.

Results and Discussion

Figure 3

Figure 3 shows high resolution HAADF STEM images of two platelets viewed edge on. The two platelets (Platelet A and Platelet B) shown are representative of the platelet core[#] structures seen in all platelets imaged. Two distinct atomic arrangements were observed and this provides direct evidence of the anisotropic structure of the platelets with Platelet A representing the atomic arrangement when viewed along $[110]_p$ and Platelet B the atomic arrangement when viewed along $[1-10]_p$.

The atomic arrangement seen for Platelet A shows a set of interstitial atoms parallel to a $(001)_p$ plane similar to that found in the Lang based models. However, high magnification images (Figure 4 and 5)

[#] In this work the “core” refers to the atomic arrangement of the platelet at its centre not including the atomic structure at the periphery where the platelet terminates in the host diamond lattice

show that the atomic configuration of Platelet A exhibits subtle displacements of the central atom from the defect midpoint in both directions. The stacking seen is not periodic along the defect line but consists of randomly staggered interstitial atoms along the defect midpoint (Figure 4). This is consistent with the zig-zag model proposed by Barry et al. (1985)¹⁰ where the position of the central interstitial atom is arranged in an inverse but equivalent position to the atomic configuration of the Lang model. This finding is further supported by the atomic arrangement for Platelet B (Figure 3) where two interstitial and less dense rows of atoms are staggered or alternated along the defect central line, also consistent with the zig-zag model.

Qualitative comparison of the experimental images to simulations using the structural models considered are shown in Figure 4.

Figure 4

Direct measurement of the lattice displacement vector $\langle f00 \rangle \{100\}$ was performed giving an average value of $f=0.33$, which is in agreement with the structure of the zig-zag model (Figure 5). No evidence for any preferential arrangement of N could be elucidated from the images acquired.

Figure 5

Several previous studies have reported that platelets are sensitive to electron beam irradiation^{15,16}. Evidence of this was observed during imaging of several platelets, where an apparent widening of the platelet core was observed over time.

To investigate this further, platelets were also imaged at lower accelerating voltage (80 kV) in order to minimize the influence of electron beam damage on the platelet structure. Figure 6 (top right) shows HAADF STEM images of the two different platelet structures viewed edge on along a $\langle 110 \rangle$ direction acquired at 80 kV.

Figure 6

The platelet structure observed in these images is consistent with that of previously reported images acquired at 200 kV. Closer inspection of the atomic arrangement of Platelet A (Figure 6) shows distinct groupings of atoms away from the defect midpoint (indicated by red lines) consistent with the zig-zag model. Interestingly, this arrangement appears to be periodic in this image similar to the findings of Barry et. al (1985)¹⁰. This might indicate an additional relaxation of atomic positions.

To investigate the presence, distribution and coordination environment of N in the platelets high spatial resolution EELS spectrum imaging across the platelets was performed. Care was taken to use probe conditions that would have sufficient flux for accurate signal detection but at the same time would not lead to progressive electron beam induced damage of the platelet structure. Figure 6 (Top Left) shows a typical core loss EEL spectrum at the C-K and N-K edge positions obtained on and off the platelet line showing clear evidence for the presence of N within the defect.

Figure 6 (bottom) shows generated signal fit coefficient maps of N, π^* bonded C and diamond using multiple linear least squares (MLLS) fitting with a reference N-K edge, π^* bonded C-K (pre-edge) and diamond C-K spectra to a typical EELS spectrum image obtained across the platelet. The fit coefficient map provides a correlation value between the reference spectrum and the experimental spectrum for

a defined energy range. For the diamond reference signal, a reference spectrum was selected from the diamond matrix

From the fit coefficient maps obtained it is clear that N is present and confined within the defect core. However, no conclusive evidence of preferential arrangement of N within the defect core was observed due to the N signal being delocalized. There may be several reasons for the observed delocalization of the N signal. Firstly, the inelastic delocalization for the imaging conditions used (convergence angle $\alpha = 20$ mrad; detector acceptance angle $\beta = 50$ mrad) is expected to be between 0.1 and 0.2 nm for a single atom N-K edge²¹. In addition, there were observed electron beam induced damage effects, evident as a modification of the defect core over time at 200 kV. An example of this is seen in Figure 6 indicated by the red arrow. Finally, the determined value of the N content in the platelet cores ranged between 5 and 8 atomic percent and hence the platelet core structure is still largely C with only a few N atoms per atomic column. This will have a pronounced effect on the N-K edge signal to noise ratio per spectrum image pixel especially taking into account the short dwell times used during acquisition to minimize the effects of electron beam damage.

The EELS signal from the defect core was found to deviate from the reference diamond spectrum. The fit-coefficients obtained from the MLLS indicated a correlation between the reference diamond EELS spectrum and the experimental EEL spectra taken from the platelet core of less than 70% (Figure 6). The deviation of spectra from the defect core compared to that from a pure tetrahedral bonding environment is also evident in the core loss spectrum of the C-K edge taken on the platelet compared to the reference bulk material (Figure 6). The presence of a distinct pre-edge peak at the edge onset is observed together with a flattening and rounding of extended edge features compared to the bulk EEL spectrum. Some diamond characteristics remain in the spectrum structure which may be due to the bonding arrangement of the C atoms at the interface region between the bulk diamond and the defect. The pre-edge peak observed is typical for a π^* bonding configuration²² which suggests a graphitic environment of C atoms in the defect core²². The MLLS fit-coefficient map obtained using the π^* pre edge peak of a graphitic C-K edge supports this, with an increased correlation seen at the defect core.

Figure 6 (bottom left) shows an average spectrum of the N-K edge within the defect core obtained by stacking and averaging all spectra containing a defect core N-K edge (1804 spectra) within 8 different spectrum images obtained across the core of 4 platelets. Averaging was carried out in order to improve the signal to noise ratio of the N-K edge. The N-K edge structure measured is similar to that of the C-K edge spectrum of the defect core with the same edge onset pre-peak present (396 eV) at the N-K edge as that observed for the C-K edge. The average signal to noise ratio for this peak is of order 3:1.

The change in the EELS structure of the C-K edge at the defect core together with its similarity to the N-K edge indicates that both atomic species co-exist in the defect core in an interstitial arrangement. Furthermore, the presence of a pre-edge feature in both C-K and N-K edges is indicative of trigonal distortion²³ of the lattice with the consequent coordination environment of the interstitial atoms being three-fold rather than four-fold. This is also consistent with the arrangement of interstitial atoms in the zig-zag structure proposed by Barry et al. (1985)⁹.

From these findings, it is clear that the basic building block of platelets in type 1a diamond structure is dependent on the presence of both C-C and C-N interstitial complexes. Such complexes would also need to contain interstitial C and N in trigonal coordination and would have to order in a staggered arrangement over several nanometres to form the platelet.

An example, of how such an arrangement could be possible, can be seen in the recent discovery of the WAR9 and WAR10 N interstitial defect complexes.²⁴ These defect complexes exhibit many characteristics similar to those in the platelets. In essence, the progression from the WAR9 to WAR10 structures can be viewed as the addition of a single staggered step in the WAR9 structure through the addition of an interstitial C atom. This constitutes a single building block for the proposed zig-zag platelet structure and provides insight into how small amounts of N can be incorporated within the platelet structure.

Conclusions

We have shown the first experimental data of the atomic arrangements in platelet defects in natural type Ia diamond. A qualitative match to the zig-zag structure model proposed by Barry et al. (1985)¹⁰ with an anisotropic atomic arrangement at the platelet core when viewed along $\langle 110 \rangle$ directions was observed. This was further supported by the fine structure in experimental EELS of C-K and N-K edges obtained from the platelet core. Spectral features supporting the presence of bonds with three-fold coordination were found, in contradiction to some earlier findings^{16,17}.

The amount of N detected in the platelet core in this study was between 5 and 8 atomic percent and no clear evidence for any preferred atomic position of N in the platelet was found. However, imaging the platelet at reduced accelerating voltage did show evidence for periodicity in the staggered arrangement indicating N ordering (supplementary information). It is clear however that the presence of interstitial C is also necessary within the platelet structure. Overall, our findings support an interstitial aggregate model of formation for the platelet defects.

References

1. Gainutdinov, R.V., Shiryaev, A.A., Boykoc, V.S. and Fedortchouk, Y. Extended defects in natural diamonds: An Atomic Force Microscopy investigation. *Diamond & Related Materials* 40, 17–23 (2013)
2. Wort, C.J.H. and Balmer, R.S. Diamond as an electronic material. *Materials Today* 11, 22-28 (2008)
3. Dhomkar, S., Henshaw, J., Jayakumar, H. and Meriles, C.A. Long-term data storage in diamond. *Science Advances* 2, e1600911 (2016)
4. Bosak, A., Chernyshov, D., Krisch, M. & Dubrovinsky, L. Symmetry of platelet defects in diamond: new insights with synchrotron light. *Acta Cryst. B* 66, 493-496 (2010).
5. Goss, J.P., Briddon, P.R. and Papagiannidis, S. Interstitial nitrogen and its complexes in diamond *Phys. Rev. B* 70, 235208 (2004)
6. Raman, C. V. & Nilakantan, P. *Proc. Ind. Acad. Sci. A* 11, 389–397 (1940)
7. Evans, T. & Phaal, C. Imperfections in type I and type II diamonds. *Proc. R. Soc. A* 270, 535–552 (1962).
8. Sobolev, E. V., Lisoivan, V. I. & Lenskaya, S. V. *Sov. Phys.-Doklady* 12, 665–668 (1968)
9. Goss, J. et al. Extended defects in diamond: The interstitial platelet. *Phys. Rev. B* 67, 165208 (2003).
10. Barry, J., Bursill, L. & Hutchison, J. On the structure of $\{100\}$ platelet defects in type Ia diamond. *Phil. Mag. A* 51, 15-49 (1985).
11. Lang, A. A proposed structure for N impurity platelets in diamond. *Proc. Phys. Soc.* 84, 871-876 (1964).
12. Humble, P., Mackenzie, J. & Olsen, A. Platelet defects in natural diamond. I. Measurement of displacement. *Phil. Mag. A* 52, 605-621 (1985).

13. Miranda, C., Antonelli, A. & Nunes, R. Stacking-Fault Based Microscopic Model for Platelets in Diamond. *Phys. Rev. Letts.* 93, 265502(2004).
14. Bursill, L. A. & Glaisher, R. W. Aggregation and dissolution of small and extended defect structures in type Ia diamond. *Am. Min.* 70 (5-6) 608-618 (1985)
15. Berger, S. & Pennycook, S. Detection of N at {100} platelets in diamond. *Nature*, 298, 635-637 (1982).
16. Fallon, P., Brown, L., Barry, J. & Bruley, J. N determination and characterization in natural diamond platelets. *Phil. Mag. A* 72, 21-37 (1995).
17. Bruley, J. Detection of N at {100} platelets in a type IaA/B diamond. *Phil. Mag. Letts.* 66, 47-56 (1992).
18. Kiflawi, I., Bruley, J., Luyten, W. & Van Tendeloo, G. 'Natural' and 'man-made' platelets in type-Ia diamonds. *Phil. Mag. B* 78, 299-314 (1998).
19. Cowley, J.M. and Moodie, A.F. The scattering of electrons by atoms and crystals. I. A new theoretical approach. *Acta Cryst.* 10, 609-619 (1957)
20. Stadelmann, P.A. An integrated set of computer programs for processing electron micrographs of biological structures. *Ultramicroscopy*, 21, 131 (1987)
21. Cosgriff, E.C., Oxley, M.P., Allen, L.J., Pennycook, S.J. The spatial resolution of imaging using core-loss spectroscopy in the scanning transmission electron microscope. *Ultramicroscopy* 102, 317–326 (2005)
22. Egerton, R. F. *Electron Energy-Loss Spectroscopy in the Electron Microscope* 2nd edn, Plenum, (1996)
23. Brydson, R. Brown, L.M. & Bruley, J. Characterizing the local N environment at platelets in type IaA/B diamond. *J. Microsc.* 189, 137-144 (1998).
24. Felton, S. et al. Electron paramagnetic resonance studies of N interstitial defects in diamond. *J. Phys. Cond. Mat.* 21, 364212 (2009).
25. Sawada, H., Shimura, N., Satoh, K., Okunishi, E., Morishita, S., Sasaki, T., Jimbo, Y., Kohno, Y., Hosokawa, F., Naruse, T., Hamochi, M., Sato, T., Terasaki, K., Suzuki, T., Terao, M., Waki, S., Nakamichi, M., Takano, A., Konod, Y. & Kaneyama, T. Super High Resolution Imaging with Atomic Resolution Microscope of JEM-ARM300F. *JEOL News*, 49, 51-58 (2014)
26. Zemlin, F., Weiss, K., Schiske, P., Kunath, W. & Hermann, K.H. Coma-free alignment of high resolution electron microscopes with the aid of optical diffractograms. *Ultramicroscopy*, 3, 49-60 (1978).
27. Kilaas, R. Optimal and near-optimal filters in high-resolution electron microscopy. *J. Microsc.* 190, 45-51 (1998).
28. de la Peña, F., Ostasevicius, T., Fauske, V.Y., Burdet, P., Jokubauskas, P., Nord, M., Chang, H. (2017). *hyperspy/hyperspy v1.2* [Data set]. Zenodo. <http://doi.org/10.5281/zenodo.345099>
29. <http://www.gatan.com/> Company page of Gatan Inc., the source of DigitalMicrograph. You can request the free license from this page and download the latest version
30. Ahn, C.C. and Krivanek, O.L. *EELS Atlas: A Reference Collection of Electron Energy Loss Spectra Covering All Stable Elements*. GATAN (1983)
31. Bursill, L., Barry, J.C, Hudson, P.R.W. Fresnel diffraction at (100) platelets in diamond: An attempt at defect structure analysis by high-resolution (3 Å) phase-contrast microscopy. *Phil. Mag. A* 37, 789-812 (1978)
32. Goss, J., Briddon, P., Jones, R. & Heggie, M. Platelets and the $\langle 110 \rangle$ a 0/4 {001} stacking fault in diamond. *Phys. Rev. B* 73, (2006).

Acknowledgements

EJO, JHN, REK, SRN wish to acknowledge the financial support of the NRF and DST in South Africa and the DST-NRF Centre of excellence in strong materials at the University of the Witwatersrand. AIK acknowledges financial support from EPSRC and the Royal Society.

Author Contributions

EJO performed the (S)TEM and EELS characterization, (S)TEM simulations and data processing. CSA, HS and EJO performed the (S)TEM imaging at 80kV. SRN provided the specimen for analysis. REK assisted in the construction of structural models used for simulation. JHN, SRN, AIK and PVA assisted in the interpretation of results. All authors contributed to writing the manuscript.

Materials and Methods

Sample Preparation

A focused ion beam (FIB) instrument was used to prepare a lamella for TEM analysis from the polished surface of a diamond disc prepared from the source material (as received).

The FIB microscope used was a FEI Helios 650 Nanolab fitted with a Ga ion beam source for milling and polishing and a gas injection system utilizing a C precursor gas for attachment of the lamella to the grid. Special care was taken during thinning and polishing (500V final step) of the lamella to avoid any beam induced damage of the specimen.

Characterization

HAADF STEM images together with EELS spectrum imaging was carried out at 200 kV accelerating voltage for most of the study reported but 80 kV imaging was also used to investigate possible effects of electron damage on the platelet structure. Conventional High Resolution TEM (HRTEM) images were also recorded (Fig. 12 -14 in Supplementary info).

Platelets in the prepared lamella were characterized using several aberration corrected instruments. The first was a double aberration (CEOS CESC/CETCOR) corrected JEOL ARM 200F fitted with a Schottky field emission electron source; secondly, a probe corrected JEOL ARM 200CF with a 5th order CEOS DCOR probe corrector both operated at 200kV. Finally a double 5th order corrected JEOL ARM300CF with eta correctors²⁴ was used for imaging at a lower accelerating voltage (80 kV). EELS spectrum imaging was carried out using a Gatan Quantum 965 ERS image filter and HRTEM images were recorded on a Gatan Ultrascan 1000 XP camera with a detector area containing 2048 X 2048 pixels with a size of 14 μm .

Image Simulation

High resolution TEM and STEM images were qualitatively compared to simulated images generated from the structural models proposed by Lang et al. (1964)¹¹, Humble et al. (1985)¹², Bursill et al. (1981)¹⁴, Miranda et al. (2004)¹³ and Barry et al. (1985)⁹ using the multislice¹⁸ method implemented in the JEMS¹⁹ image simulation program.

In the current study the foil thickness was estimated through the use of a Kramers-Kronig analysis²² using the EELS low loss region around the platelets giving a typical thickness of 15-30 nm. The aberration coefficients were measured from a Zemlin tableau²⁶ recorded during fine tuning of the (S)TEM corrector before analysis using an amorphous C region present on the FIB section. Image simulations for TEM and STEM images were done using the following parameters.

Table 1 – Multislice simulation parameters used for TEM and SEM images.

| | α | A_2 | B_2 | A_3 | C_s | C_c | C_5 | Δt (foil thickness) | ΔE | Slices (0.255nm) |
|------|----------|-------|-------|--------|-------------|--------|---------------|-----------------------------|------------|------------------|
| TEM | 7.6 mrad | 12 nm | 33 nm | 265 nm | 3.5 μm | 1.2 mm | 18 μm | 25 nm | 0.9 eV | 98 |
| STEM | 20 mrad | 24 nm | 29 nm | 201 nm | 3.2 μm | 1.2 mm | - 1,144 mm | 15 nm | 0.9 eV | 58 |

STEM Image processing

STEM images were filtered to remove high frequency noise using a Fourier filter developed from the work of Kilaas (1998)²⁷ and implemented in a Digital Micrograph script due to Mitchell (www.dmscripting.com). Raw data corresponding to Figure 3 is shown in the Supplementary Information.

EELS Spectrum Image Processing

EELS spectrum imaging data was denoised using principle component analysis as implemented in Hyperspy²⁸. The data was decomposed into 20 factor components and reconstructed using typically 3 or 4 principle components identified.

The MLLS fitting was carried out using the built in MLLS routine in GATAN Digital Micrograph²⁹ with the fit-weights set equal to one in both cases. For the diamond reference signal, a reference spectrum was selected from the diamond matrix. The N-K reference signal was extracted from the EELS Atlas³⁰ provided with the Digital Micrograph (Gatan Microscopy Suite) software. The π^* bonded C-K signal was extracted from a reference EELS spectra of graphite obtained from a reference specimen. The fit range for the diamond signal was set between 280 eV and 350 eV energy loss. The fit range for the N-K signal was set between 370 eV and 440 eV energy loss. The fit range for the π^* bonded C was set between 280 eV and 285 eV.

The quantification of the relative N content at the platelet core was done using the quantification routine provided in the Digital Micrograph software. The quantification routine in the software implements the theory formulated in Egerton²² p277-283 for a finite integration range. The formulation is based on the relationship²²

$$I_k = NI\sigma_k$$

where N is the areal concentration (atoms / nm²) of the atoms giving rise to the ionization edge k, I_k is the sum of all counts in that edge (without background), I is the total integrated number of counts, and σ_k is the cross-section for ionization of an electron in the associated shell. The cross section used for the N-K and C-K edges was that calculated from the Hartree Slater model and a power law background fitting was used.

Figures

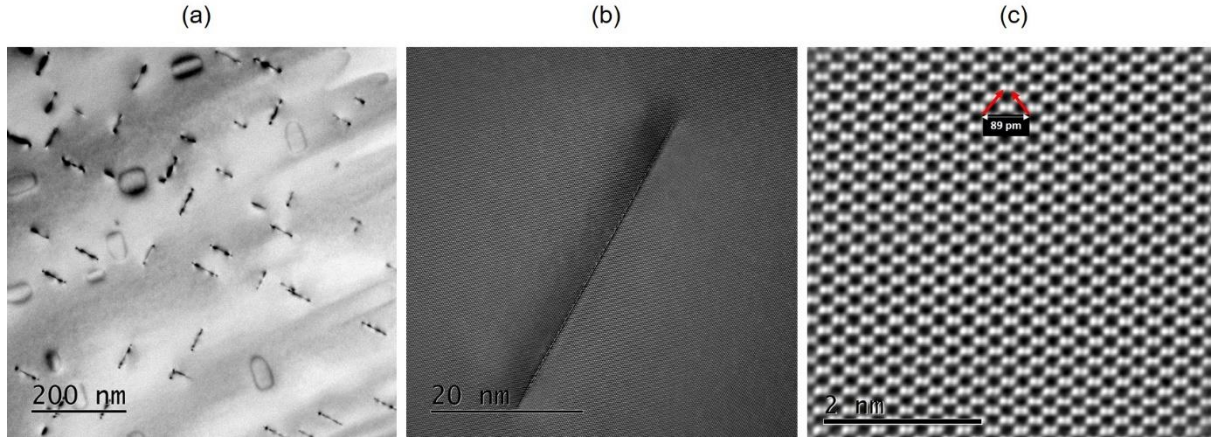


Figure 1. (a) Bright field TEM image of platelets in diamond. The platelets on $(100)_p$ and $(010)_p$ planes are viewed edge-on and loops on inclined $\{111\}$ planes are also visible. (b) High resolution TEM image showing a single platelet. The beam direction is parallel to $\langle 110 \rangle$ (c) HAADF STEM image of diamond viewed along an $\langle 110 \rangle$ beam direction showing the 89 pm $\{004\}$ separation.

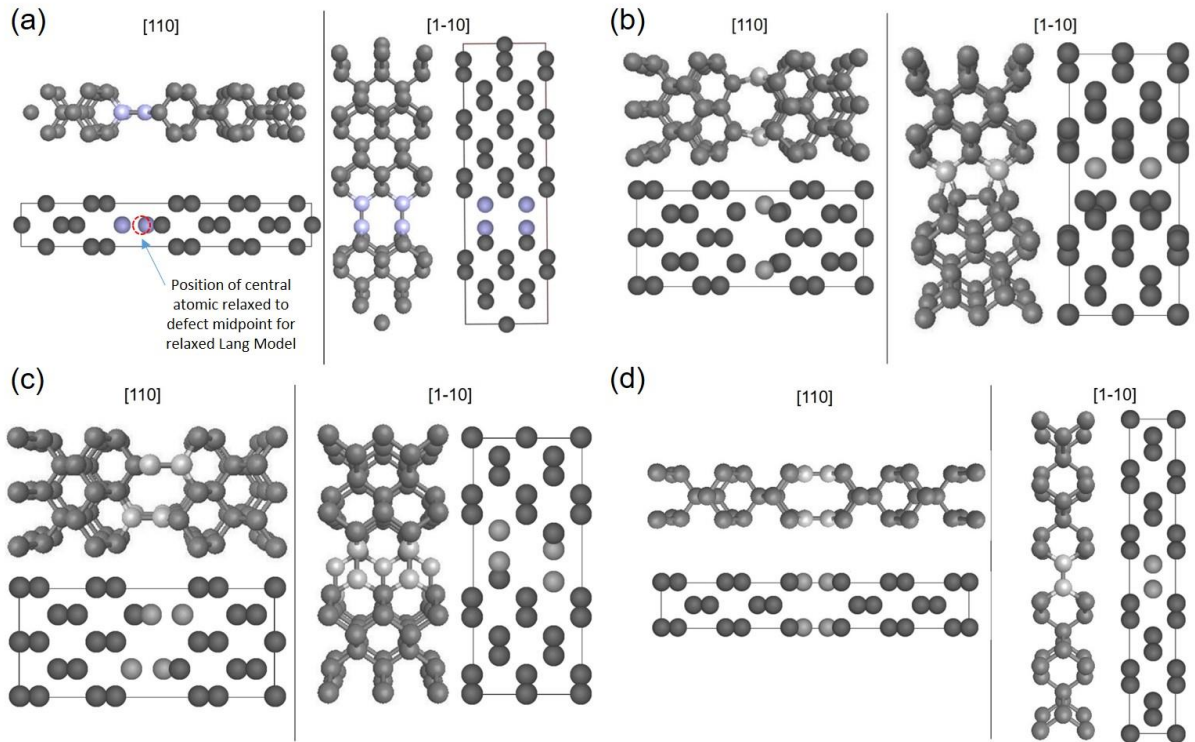


Figure 2. (a) Atomic structures of the Lang and relaxed Lang models viewed along $[110]_p$ and $[1-10]_p$ directions. Blue spheres represent the interstitial layers containing N^{10,13}. (b) Atomic structure of the Humble model viewed along the $[110]_p$ and $[1-10]_p$ directions¹¹. The light grey spheres represent the position of interstitial C in the defect arrangement. (c) Atomic structure of the zig-zag model viewed along the $[110]_p$ and $[1-10]_p$ directions⁹. The light grey spheres represent the interstitial/substitutional atomic sites within the defect core. The interstitial/substitutional sites contain N or C atoms. (d) Atomic

structure of the Miranda model viewed along the $[110]_p$ and $[1-10]_p$ directions. The light grey spheres represent the interstitial sites within the defect core¹².

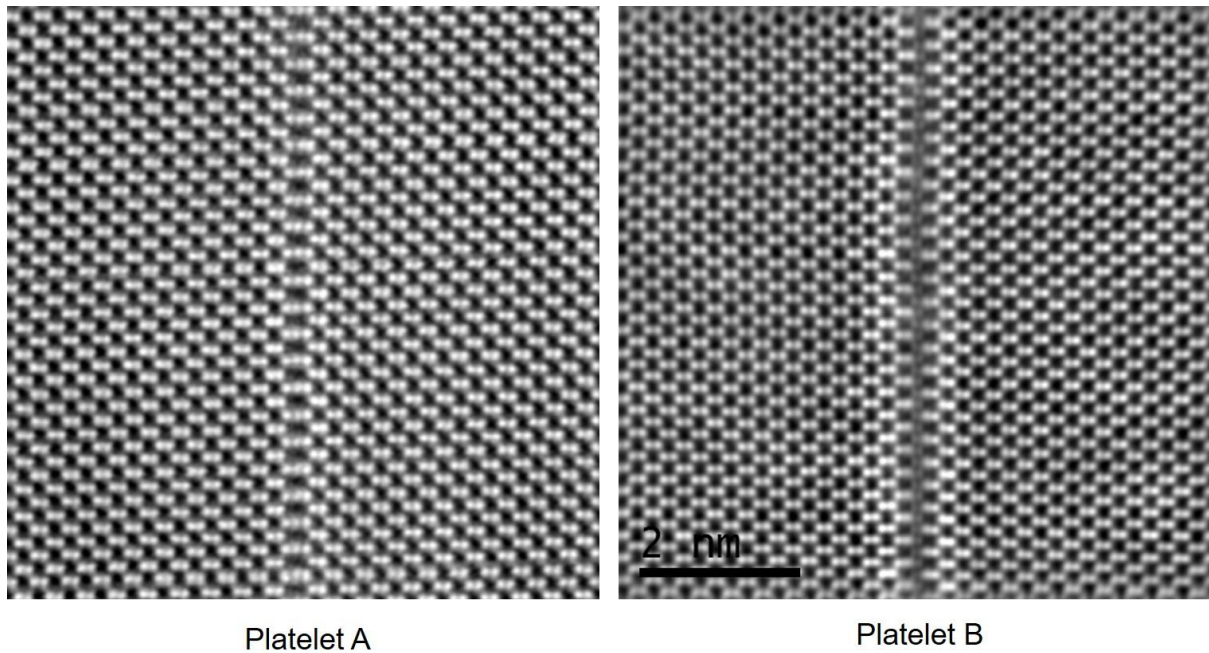


Figure 3. High resolution HAADF STEM images of two platelets viewed edge-on along $\langle 110 \rangle$ directions showing the asymmetric nature of the platelet structure. Each image has a pixel array of 512×512 (pixel size = 0.014 nm) and is an average of five summed frames. (Pixel dwell time = 16 μ s; beam convergence semi-angle α = 20 mrad; detector acceptance semi-angle β = 68-280 mrad; probe size < 0.1 nm). Equivalent raw data is shown in Supplementary Information.

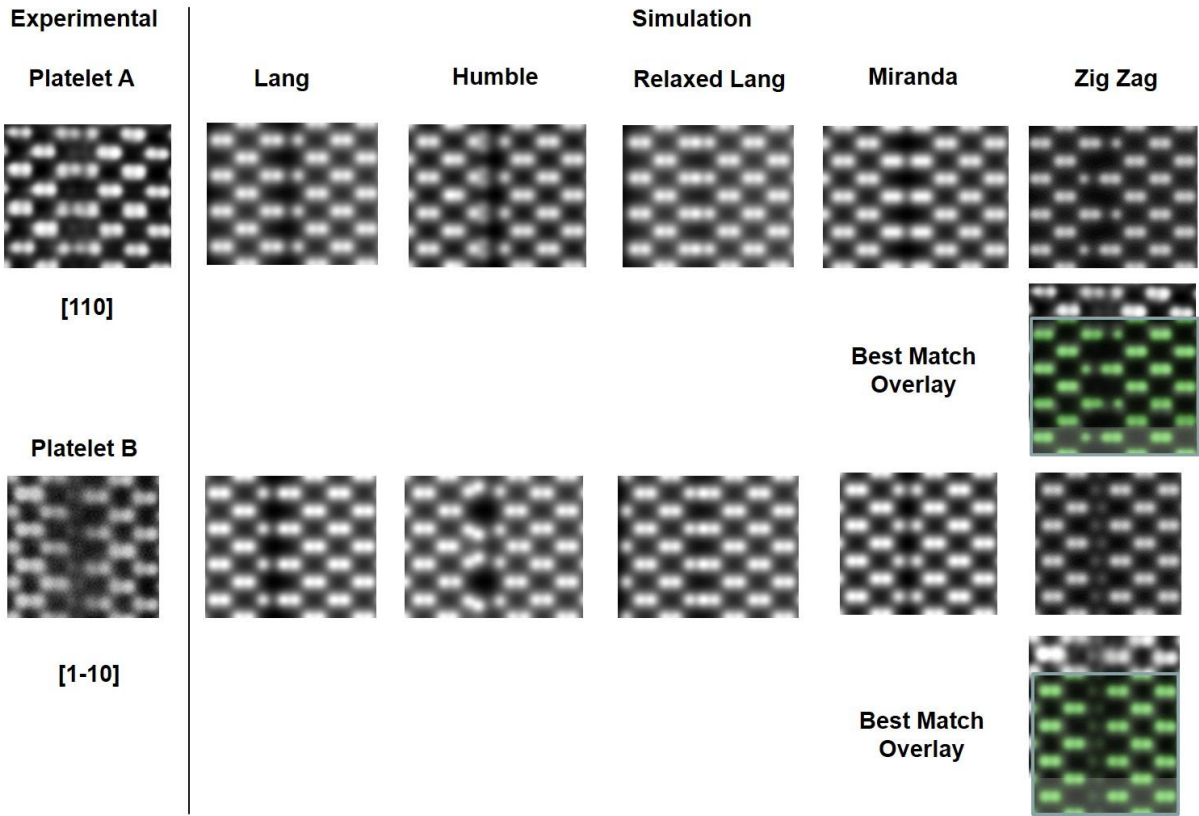


Figure 4. Qualitative comparison of experimental HAADF STEM images of platelet A and B to multislice simulations of the platelet viewed along the $[110]_p$ and $[1-10]_p$ directions using the selected platelet structure models. The overlay in green shows the simulated image for the best-matched structure. ($\alpha = 20$ mrad; $A_2 = 24$ nm; $B_2 = 29$ nm; $A_3 = 201$ nm; $C_s = 3.2$ μ m; $C_c = 1.2$ mm; $C_5 = -1,144$ mm; $\Delta t = 25$ nm; $\Delta E = 0.9$ eV). An overlay (in green) of the simulated image for the best-matched structure model to experimental image is also shown.

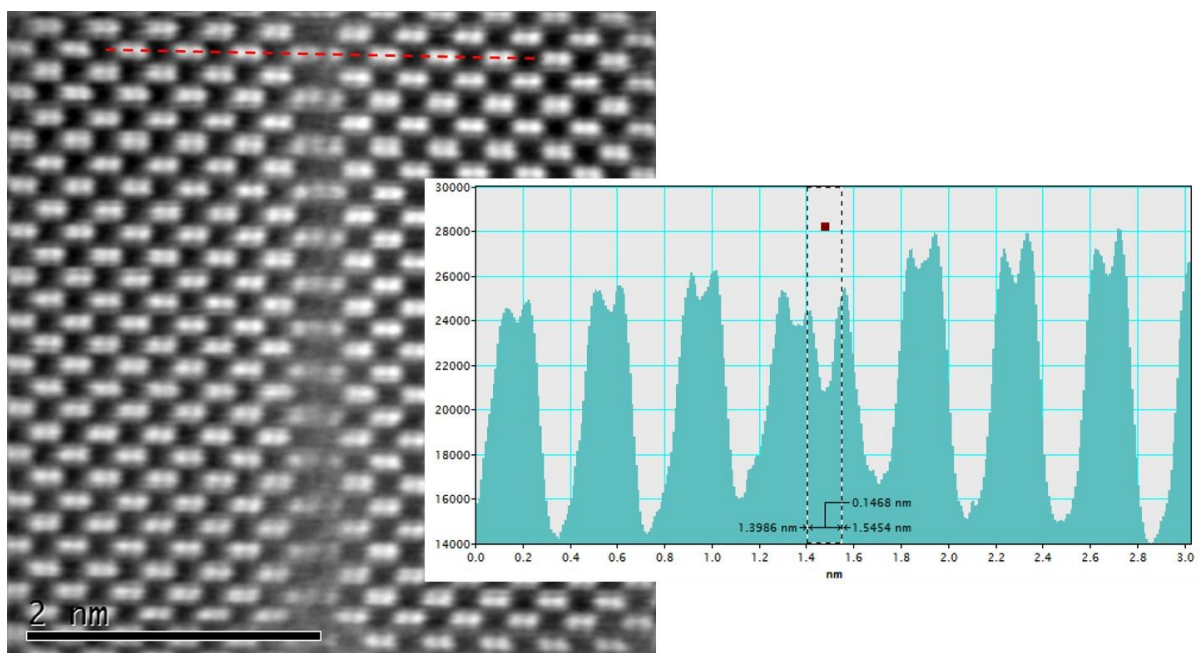


Figure 5. Higher magnification HAADF STEM image of Platelet A, together with a line profile across the platelet core indicated by the red dotted line.

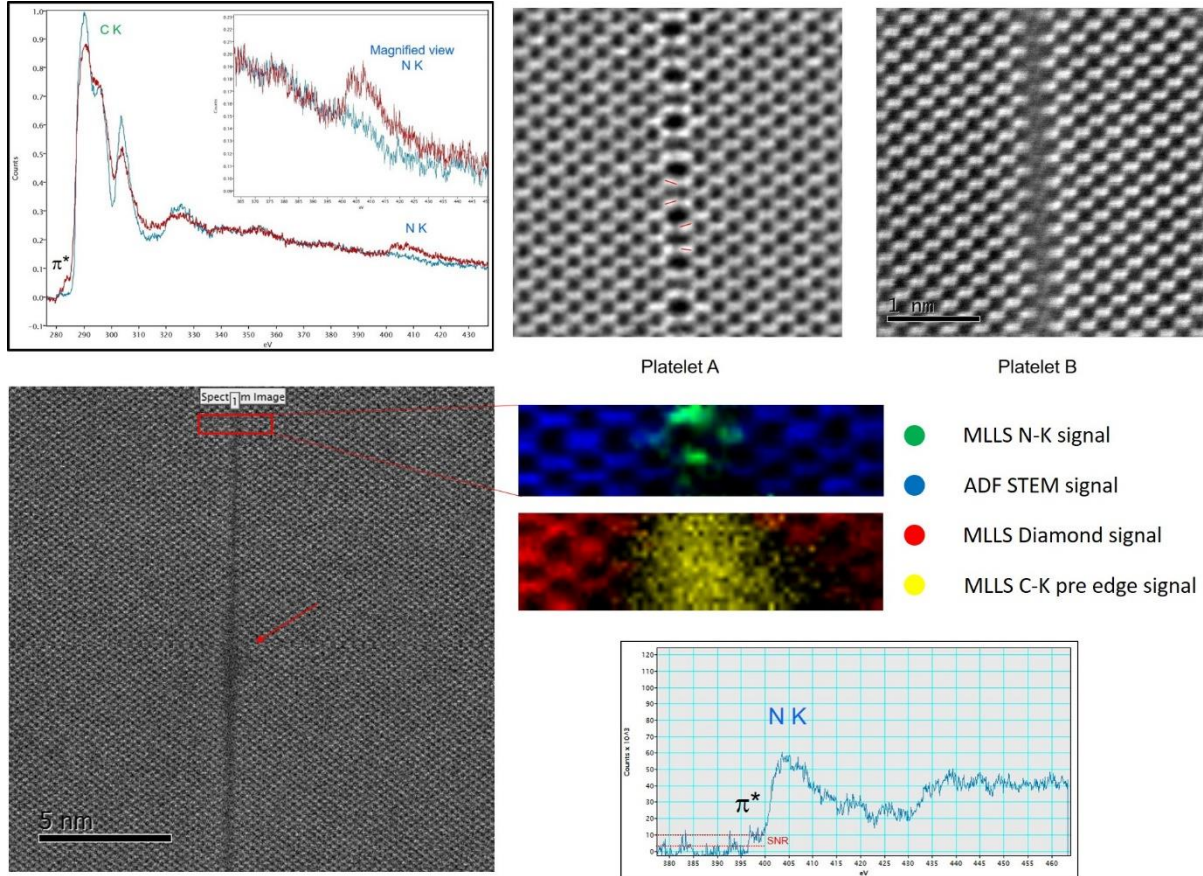


Figure 6. (Top right) High resolution HAADF STEM images of two platelets viewed edge on along $\langle 110 \rangle$ directions, imaged at 80 kV accelerating voltage. Each image has a pixel array of 1024x1024 (pixel size = 0.003 nm) and is an average of five summed frames. (Pixel time = 20 μ s; α = 20 mrad; β = 68-280 mrad) (Top left) Core loss electron energy loss spectra obtained on (red) and off (blue) the platelet for C-K and N-K edges. Inset is a magnified view of the N-K edge. Typical experimental parameters were; probe size < 0.1 nm, probe current density < 68 pA, convergence angle 20 mrad, spectrometer acceptance angle ca. 50 mrad, accelerating voltage 200kV. (Middle right) Results from MLLS fitting across the platelet core using reference N-K and C-K core loss edges. HAADF STEM image of the spectrum image area in blue with N signal in green. Fit coefficient maps of diamond reference C-K signal in red and π^* pre edge of C-K signal in yellow. (Bottom left) Survey image indicating the area from which the spectrum image was obtained (indicated by the red box). The red arrow shows a region of the platelet core that experienced electron beam damage due to prolonged exposure to the electron beam. (Bottom Right) Power law background subtracted averaged core-loss N-K edge obtained from stacking and averaging 1804 core-loss edges obtained from the cores of 4 platelets in 8 spectrum images. A pre edge feature at 396 eV energy loss is seen with an average signal to noise ratio of 3:1